

## Electrical and corrosion characterisation of nano-composite eutectic Bi-Ag solder alloy reinforced with multi-wall carbon nanotube and multi-layer graphene

Nima Ghamarian<sup>1</sup>, M.A Azmah Hanim<sup>1,2\*</sup>, Zulkarnain Zainal<sup>3</sup>, Lim H.N<sup>3</sup>

### Affiliations:

<sup>1</sup> Department of Mechanical and Manufacturing Engineering, Faculty of Engineering Universiti Putra Malaysia, 43400 Serdang, Selangor, Malaysia

<sup>2</sup> Research Center Advance Engineering Materials and Composites (AEMC), Faculty of Engineering, Universiti Putra Malaysia, 43400 Serdang, Malaysia

<sup>3</sup> Department of Chemistry, Faculty of Science, Universiti Putra Malaysia, 43400 Serdang, Selangor, Malaysia

\*Corresponding author: M.A Azmah Hanim<sup>\*</sup>, Department of Mechanical and Manufacturing Engineering, Faculty of Engineering Universiti Putra Malaysia, 43400 Serdang, Selangor, Malaysia.

Received: September 09, 2020 Published: October 28, 2020

### Abstract:

Bi-Ag solders were proposed in this research as alternative to high lead solder. In order to improve its property, reinforcement with multi wall carbon nanotubes (MWCNT) and multi-layer graphene (MLG) were proposed. The electrical and corrosion characterisation of the nano-composite eutectic Bi-Ag lead free solder were evaluated in this research. The nano-composite samples were made by using powder metallurgy technique. It is found that for both reinforced nano particles in the matrix, the electrical resistivity decreased, while the effect of MWCNT on the electrical resistivity of the solder matrix was more than MLG. The corrosion behavior of Bi-2.5Ag and its composite samples with MWCNT and MLG was studied by an electrochemical technique. The results from Tafel plot curves which were run in three different acidic electrolytes illustrated that the corrosion rate for all the composite samples increased. Furthermore, it was deduced that the corrosion rate and passivation were the functions of the electrical conductivity of the sample, the electrical conductivity of electrolyte and the number of H<sup>+</sup> in the corrosive electrolyte.

**Keywords:** Lead free solder, nano-composite solder, electrical characterisation, corrosion characterisation, eutectic Bi-Ag, MWCNT, MLG

### 1. Introduction

The past few decades have seen foremost progress in soldering materials and alloys for electronics assembly technologies due to the replacement of tin-lead with lead-free soldering alloys. Regarding the environmental consideration, the elimination of lead (Pb) from electronic solder alloy was first proposed in the early 1990s by US legislation [1,2]. Thus, a critical analysis of interconnection components and alloys development from composite solder alloys and a comprehensive evaluation of the solder joints with the plain solder alloy are important to the quest of finding a more reliable and operational alternative to existing solder alloy candidates [3, 4].

However, with the miniaturization of electronic gadgets and the usage of IC terminals, critical assessment of the lifetime operational capability in interconnection joints must have the highest concern.

Hence, reliability inspection issues associated with the development of the lead-free solder candidates is a necessity [5]. In the recent times, heat generation and thermal conductivity in electronic devices which were used in aerospace, automotive, militaries, nuclear power facilities and monitors initiate the need of high temperature lead free solder [6-9]. Some elements such as gold (Au), zinc (Zn), bismuth (Bi) and tin (Sn) have been suggested to replace Pb and produce lead free soldering alloys for high temperature applications [10-12].

Among all suggested high temperature lead free solder alloys, Bismuth-Silver Alloys (Bi-Ag) provides improve features for different applications [13]. It can be concluded from the Bi-Ag phase diagram that a binary system contains only one eutectic reaction, which occurs at 97.5% Bi and at a temperature around 262.5 °C.

There are no intermetallic parts, and the low solubility of silver in bismuth precludes a solid-solution establishment. The presence of the silver element in the microstructure makes Bi-Ag alloys mechanically stronger and more ductile than pure bismuth [14]. The reliability and applicability of Bi-Ag solder alloy in industries need further investigations considering their advantages and disadvantages. Thus, the investigations to improve the durability properties of these alloys are ongoing [15-18].

Studies have shown that adding alloying elements frequently improves the properties of alloys [19-25]. It is reported that Sn-Ag-Cu solder reinforced with multiwall carbon nanotube considerably improved the electrical properties of solders. The experimental results showed samples with CNT have a better thermal performance. This is the effect of lower coefficient of thermal expansion (CTE) values [26]. Also, the influence of adding CNT on silver-filled electrical conductivity has been investigated. The result illustrated that CNT improved the electrical conductivity. For example, the electrical resistivity of the samples, which had 66.5 wt% silver conductive adhesive with no CNT gives a value of 104  $\Omega\text{cm}$ , but after adding 0.27 wt% CNT, the resistivity decreased to  $10^3 \Omega\text{cm}$ . Hence, adding CNT to the interconnecting adhesive components such as solder alloys can vastly improve electrical properties and mechanical properties [27-29].

While according to the reinforcement of SAC alloy with graphene nano particles, it is reported that small improvement were detected in the electrical conductivity [30]. It was also mentioned that Ni coated graphene can improve the electrical conductivity of the alloy [31]. It is reported that adding graphene nano sheets (GNS) improved the corrosion resistance of the 96.5Sn-3Ag-0.5Cu solder in a 3.5 wt% NaCl electrolyte at room temperature. By increasing the GNS content to 0.03 wt%, the corrosion rate declined. Therefore, the corrosion resistance of SAC alloy with GNS is improved in comparison to the pure SAC [32].

Based on those information, it can be deduce that improvement in the characteristics of lead free solders by a proper selection of the reinforcement materials could produce better alloys due to its physical and mechanical properties. In consideration of the aforementioned facts, multi wall carbon nanotube (MWCNT) and multi-layer graphene (MLG) were selected as the reinforcement materials in the current study to compare and analyze in detail their electrical conductivity and corrosion resistance.

## 2. Experimental procedure

Powder metallurgy technique was used to produced Bi-2.5Ag and its reinforced systems (Bi-2.5Ag + xMWCNT/xMLG,  $x = 0.01, 0.03, 0.05, 0.07$  and  $0.1 \text{ wt}\%$ ). The main raw materials utilized in the experimental procedures to synthesize the lead free solders were highly pure nano powder. Multi wall carbon nano tubes specifications are 10-20 nm outer diameter, 0.5-2.0  $\mu\text{m}$  length, 95 wt% purity and contained 1.5wt% ash. Multi-layer graphene had 97 wt% purity, 2  $\mu\text{m}$  diameter, 600-750  $\text{m}^2/\text{g}$  surface area and it is classified as a third grade graphene. The Cu plates were used as substrates. The powders were mixed for 16 h with the speed of 750 rpm. After mixing, the powder was compacted with force of 105 kN to produce a solder pellet. The pellets were melted at 290  $^\circ\text{C}$  to form the solder joints prior to characterisation.

### 2.1 Electrical resistance measurement

Electrical resistance measurement of the composite metal alloys can be studied by two-probe (Multimeter). The obtained results by this method are affected by the resistance of connection points between the sample and wire. Thus, to eliminate the resistance effect of the contact point, it is suggested to use the four-point method in literature [33]. Hence, the electrical resistivity ( $\rho$ ) of bulk Bi-2.5Ag and its reinforced samples were measured by using four-point probe (Jandel model) technique. The solder pellets for this study is not melted on the copper substrate. The solder samples which were used in this measurement had a disc shape with the approximate diameter of 12 mm and the average thickness of 0.9 mm. The samples were located at the sample holder and to avoid losing current (provide a better connection between probes and sample surface) a silver paste was used at the contact points. The applied current to the sample was varied from 0.02 to 0.1 Ampere (A) and subsequently, the corresponding voltage was measured.

In general, four-point probe works based on ohm's law,  $V = IR$ , to measure the resistance. In this study, the distance between the probes is much smaller than the sample thickness. Therefore, the following equation were used to calculate the resistivity of the bulk samples at room temperature (26.5  $^\circ\text{C}$ ) [33],

$$\rho = 2\pi s \left( \frac{V}{I} \right) \quad (1)$$

where V is voltage (V), I is current (A) and  $\rho$  is the resistivity of bulk sample ( $\Omega\text{.cm}$ )

## 2.2 Electrochemical measurement

The polarization measurement was carried out by using a three-electrode cell in which electrodes were immersed in selected corrosive electrolytes. The solder bump on Cu substrate represents the working electrode (WE) and performed as a cathode in the three-electrode cell. The solder bump had a clean and shiny surface which was achieved by grinding and polishing to attain 113.0 mm<sup>2</sup> surface area (d=12mm). The sample holder allowed the corrosive electrolyte to reach the target area and its component materials (from other sides of solder bump) were not affected by the corrosive solution. The reference electrode (RE) was Ag/AgCl and the counter (CE) was a standard platinum wire. To avoid the potential junction between immersed electrodes, the three electrodes were located as close as possible. The corrosion equipment setup was fully monitored by a computer operating by Electrochemical Measurement Analysis System software. Furthermore, the corrosion measurement was controlled by AUTOLAB  $\mu$ -type III. The corrosion experiments were run at ambient temperature (26.5 °C). In order to remove the dissolved oxygen from the electrolytes, nitrogen gas was used to remove oxygen and provide an appropriate atmosphere for the corrosion experiments.

Tafel Plot measurement was performed on the samples in the supportive electrolyte by polarizing (anodic and cathode) them from the corrosion potential. For calculation, the corrosion rate, corrosion current ( $i_{corr}$ ) and corrosion potential ( $E_{corr}$ ) were extracted by extrapolating the linear parts of the polarization curves. The Tafel plot was performed with a potential speed scan rate of 20 mVs<sup>-1</sup>. The experiment was executed from the potential range of 1.0 V to -1.0 V based on the Cyclic Voltammetry (CV) results. The value of the Tafel peak on over-potential axes ( $\eta$ ) was recognized as the corrosion potential ( $E_{corr}$ ). The tangents intercept on anodic and cathodic sections of polarization curve recognized as the  $i_{corr}$  value. The value of  $i_{corr}$  is in 10 logarithmic scale on the current density axes. The mass of metal in grams which will be oxidized by the passage of one Faraday of electric charge (Q) is known as the equivalent weight (EW). The EW value is independent of the unit system and it can be considered as dimensionless. The equivalent weight for the alloy were calculated by:

$$Q = \sum \frac{n_i f_i}{W_i} \quad (2)$$

Hence,

$$EW = \frac{1}{\sum \frac{n_i f_i}{W_i}} \quad (3)$$

where  $f_i$  is the mass fraction of the  $i^{\text{th}}$  element in the alloy component,  $n_i$  is the valence electron of the  $i^{\text{th}}$  element of the alloy and  $W_i$  is the atomic weight of the  $i^{\text{th}}$  element in the alloy. Generally, only elements with the mass of above 1 percent in the alloy components were included in the calculation. In cases where the actual alloy analysis is not obtainable, it is acceptable to use the composition specification mid-range for each element. The rate of corrosion can be calculated by mathematical treatment using the approximate value of  $i_{corr}$  which was extracted from the intercepting slopes of the Tafel graph, at the anodic and cathodic sections. The corrosion rate were calculated by [34]:

$$C.R. = \frac{K \times i_{corr} \times EW}{SA \times R} \quad (4)$$

where K equals to  $3.27e^{-3}$  (mmg/ $\mu$ Acm yr),  $i_{corr}$  is known as corrosion current density ( $\mu$ A/cm<sup>2</sup>), EW is equivalent weight,  $\rho$  is density (g/cm<sup>3</sup>), and corrosion rate (C.R.) is computing in, mm/yr. The convexities located at the cathodic and anodic part of Tafel plots is related to electrochemical reaction current between the solder alloy and the corrosive electrolytes in the logarithmic value. These convexities on the Tafel plot made it hard to draw the appropriate slopes on the oxidation and reduction areas. Thus, to estimate the average value of corrosion current ( $i_{corr}$ ) and then calculate the rate of corrosion, the strategy was to draw the slope lines by using a consistent way of drawing in the cathodic and anodic parts of Tafel plot which provide the possibility of determining all the  $i_{corr}$  and then made the average with the ones situated nearby each other.

Passivity is a behavior in which an alloy or a metal displays a greater corrosion resistance from its situation in the EMF series than expected. This is a result of the formation of an extremely protective and a very thin film on a metal or alloy surface. Materials which exhibit passivity behavior are corrosion resistance in an oxidizing environment but they become chemically active in reducing environment [35]. The corrosion behavior of a metal that displays passivity can be divided into three sections located on the anodic part of the Tafel plot. These three sections are active, passive and transpassive. In the active section, the behavior of this material is identical to the general corrosion.

Indeed, a slight increase in the oxidizing of the electrolyte causes a big increase in the rate of corrosion. This increase is related to a plotting on a logarithmic scale. The oxidizing potential of the electrolyte is controlled by both the specific oxidizing power and the concentration of corrosive agents. By increasing the oxidizing agent, the corrosion rate displays a sudden decrease. This fact corresponds to the formation of the passive section. Further increase in the oxidizing agents makes a little change in the metal corrosion rate. This region is known as a transpassive region. In this region, the protective thin film does not have an opportunity to form. The set up for this experiment was similar to the Tafel experiment set up [35].

### 2.3 Corrosive electrolytes

To study the corrosion behavior of reinforced Bi-2.5Ag, the supportive electrolytes were selected as 0.5 M KCl. The 0.5 molarity was chosen to approach the maximum electrolyte conductivity [36]. Furthermore, the pH of KCl is around 6.5 which makes it suitable to control the pH with the selected acids. The supportive media was prepared using Millipore water (18 M $\Omega$ -cm) and kept for 24 hours to let the ions become hydrated. The pH of the supporting electrolyte was set as 5 by adding HNO<sub>3</sub>, H<sub>2</sub>SO<sub>4</sub> and HCl. pH 5 was chosen because most soldering flux pH, used by the packaging industry is around this pH value [37, 38]. The corrosion cell contained 200 ml of KCl. A buffer solution of the selected acid was used to prevent a change in the cell volume and KCl molarity during pH adjusting.

## 3. Results & Discussions

### 3.1 Effect of MWCNT and MLG on electrical resistance of Bi-2.5Ag

The data provided by Figure 1 illustrates the electrical resistivity of Bi-2.5Ag and the composites (for 0.01 wt% to 0.1 wt% of the reinforced nano particles in solder matrix). At the first glance, it can be found that for both reinforced nano particles in the matrix, the electrical resistivity decreased; while, the effect of MWCNT on the electrical resistivity of the solder matrix is more than MLG. This difference can be attributed to the electrical behavior, surface area and quality of each reinforcement particles which are in physical contact with each other. As illustrated, just by adding 0.01 wt% of nano particles to the matrix, the electrical resistivity of Bi-2.5Ag decreased from 3.67 ( $\mu\Omega$ .cm) to 2.38 ( $\mu\Omega$ .cm) and 2.96 ( $\mu\Omega$ .cm) for MWCNT and MLG, respectively. By increasing the weight percentage of nano particles in the matrix, the resistivity decreased with the linear trend.

The linear trend can emphasize that the reinforced Bi-2.5Ag has a composite structure and no chemical reaction occurs between its incorporator components. The maximum decrease of the resistivity was observed in the sample with 0.1 wt% of nano particles which is 1.89 ( $\mu\Omega$ .cm) for MWCNT and 2.53 ( $\mu\Omega$ .cm) for MLG.

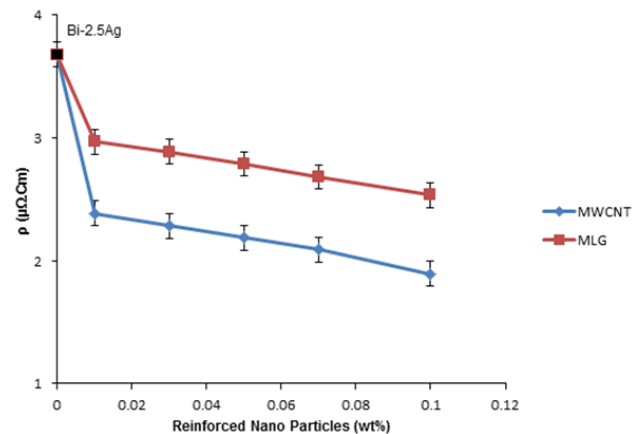


Fig 1: The effect of reinforced nano particles on the electrical resistivity of Bi-2.5Ag.

Regarding the electrical behavior of the reinforced nano particles which have metallic or semiconductor electrical characteristics, the optical absorbance of MWCNT and MLG powders was recorded between 300-600 nm light wavelengths as shown in Figure 2. The band gap energy  $E_g$  for powders as estimated by Stern equation was found around  $6.06 \times 10^{-20}$  eV and  $6.33 \times 10^{-20}$  eV for MWCNT and MLG, respectively. Indeed, the study of band gap by absorbance is an estimation because of numerous factors such as the size and shape of nano particles. The value of band gaps which was calculated from the optical absorbance characteristics of nano powders indicates that MWCNT and MLG have a metallic electrical behavior.

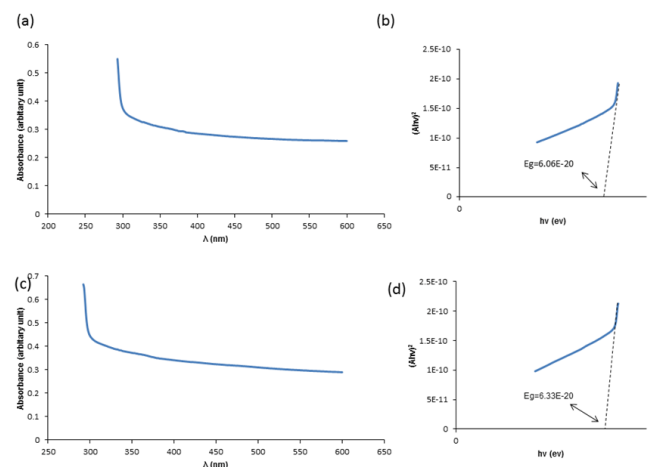


Fig 2: (a) The optical absorbance and (b) band gap energy of MWCNT are depicted (c) the optical absorbance and (d) band gap energy of MLG.

Moreover, the volume distribution of MWCNT and MLG which were shown in Figure 3, illustrates MWCNT has a smaller particle size in comparison to MLG. According to this BET experiment, it can be calculated that the specific surface area for MWCNT and MLG are  $0.432 \text{ m}^2/\text{g}$  and  $0.348 \text{ m}^2/\text{g}$ , respectively. From this extracted data, it can be deduced that while the reinforced nano particles have the same weight percentage in the matrix, MWCNT has a larger surface area than MLG. Besides, electrons on the surface of the metal or metal alloys provide an electron cloud which is involved in the electrical resistivity/conductivity [39, 40]. Thereby, MWCNT provides more opportunities for electrons to move easily in the composite solder compared to MLG.

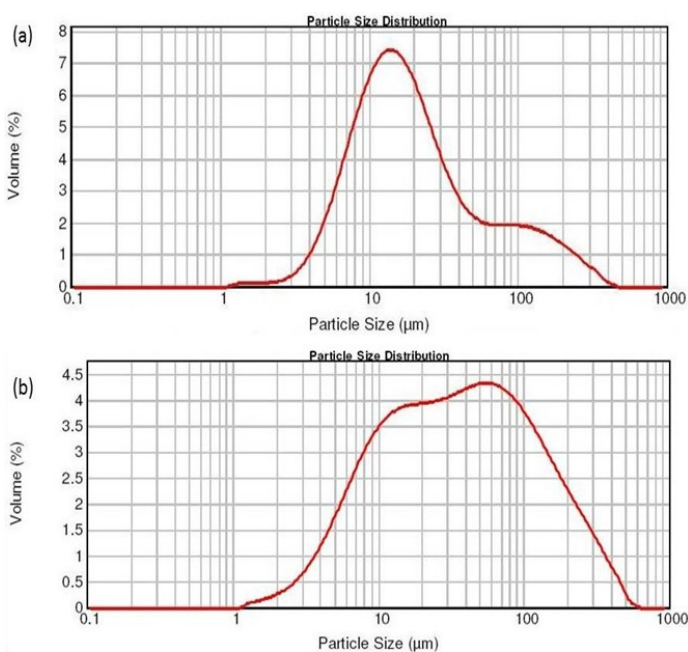


Fig 3: The distribution of volume (percentage) with respect to the nano particle size for (a) MWCNT (b) MLG.

Further investigation performed by Raman spectroscopy on MWCNT and MLG revealed the structural defects of these nano particles as it can be seen in Figure 4. The  $I_D/I_G$  ( $\approx 0.93$ ) ratio which corresponds to MLG is bigger in comparison to the  $I_D/I_G$  ( $\approx 0.54$ ) of MWCNT. This ratio represents the disruption of C=C bond which indicates structural defects and/or the presence of functional groups [41]. Hence, it can be said that MWCNT has a structure with fewer defects in comparison with MLG and it can provide a better mobility for electrons.

The 2D peak is also representing the quality of the nano particles which is the secondary D peak. Nearly, all types of  $\text{sp}^2$  carbon materials display a strong peak in the range of  $2500\text{--}2800 \text{ cm}^{-1}$  in the Raman spectra. This peak has a sharp and large intensity for a single layer carbon nano tube and graphene, but it broadens by increasing the number of layers.

This outline, in principle, could be the drawback of splitting electron bands between layers [42]. Furthermore, graphene has a multi-layer structure and due to the fact, that, by increasing the number of the layers the characteristics of graphene shift to graphite. In general, the electrical conductivity of graphite is less than the carbon nano tube.

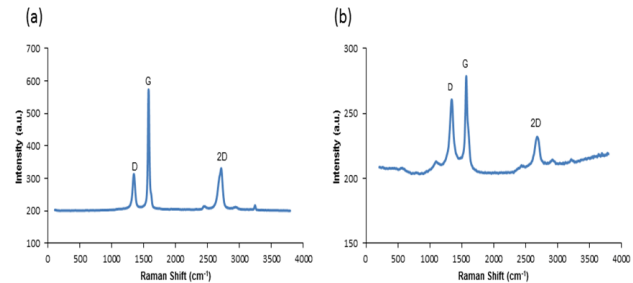
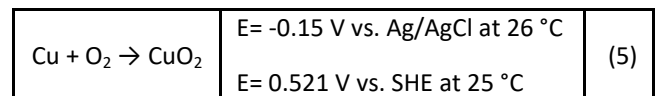


Fig 4: Raman spectra for (a) MWCNT (b) MLG

### 3.2 Effect of MWCNT and MLG on corrosion behavior of Bi-2.5Ag

#### 3.2.1 Calculation of the atomic equivalent weight for Bi-2.5Ag

Figure 5(a) display the CV related to the Cu substrate. The reduction potential value for Cu is around  $-0.15 \text{ V}$ . With the



assistance of Pourbaix diagram (Fig 6(a)), it can be deduced that the corrosion formula for Cu occurs as follows:

To find the valency of Bi and Ag and the effect of nano reinforcements on their valency, the solder alloy of Bi-2.5Ag, Bi-2.5Ag /MWCNT, Bi-2.5Ag /MLG systems were investigated by CV scheme. Figure 6 shows the CV which is related to Bi-2.5Ag, Bi-2.5Ag + 0.1 wt% MWCNT and Bi-2.5Ag + 0.1 wt% MLG. The CV figures revealed that by increasing the weight percentage of nano particles in the solder matrix, the area inside the redox reactance, the intensity of oxidation and reduction peaks increased. The increased area can be the effect of MWCNT and MLG super-capacitance characteristics. The increase in the intensity of peaks is the effect of nano particles on the electrical behavior of Bi-2.5Ag in which by increasing the amount of MWCNT and MLG in the solder matrix, the electrical conductivity improved.

The oxidation peaks belonging to Bi and Ag concealed the original element peaks. This can be the effect of scan rate or the electrolyte which CV was conducted. Hence, the suggested corrosion process for these two alloy components were assumed from their associated Pourbaix diagrams at the pH of 5, the pH of corrosive electrolytes.

From Pourbaix diagram of Bi and Ag (Fig. 6(b) and 6(c)) following formulas can be extracted:

$2\text{Bi} + \frac{3}{2} \text{O}_2 \rightarrow \text{Bi}_2\text{O}_3$	$E = 0.308 \text{ V vs. SHE at } 25^\circ\text{C}$	(6)
$2\text{Ag} + \frac{1}{2} \text{O}_2 \rightarrow \text{Ag}_2\text{O}$	$E = 0.799 \text{ V vs. SHE at } 25^\circ\text{C}$	(7)

The Bi-2.5Ag atomic equivalent weight was calculated according to equation 2, 3 and based on the thermodynamic evolutions of elements in the solder alloy (the most probable valencies which involved in the corrosion procedure). Table 1 illustrates the values according to the atomic weight; valency and the mass fraction of elements are involved in the corrosion process.

$Q = \sum \frac{n_i f_i}{W_i}$	$= [(65.96/208.9)3 + (34.03/107.8)1] = 1.2628/100 = 0.0126$	(8)
--------------------------------	---	-----

So, the atomic equivalent weight for Bi-2.5Ag and its reinforced system is:

$EW = \frac{1}{\sum \frac{n_i f_i}{W_i}}$	$= 1/0.0126 = 79.36$	(9)
---	----------------------	-----

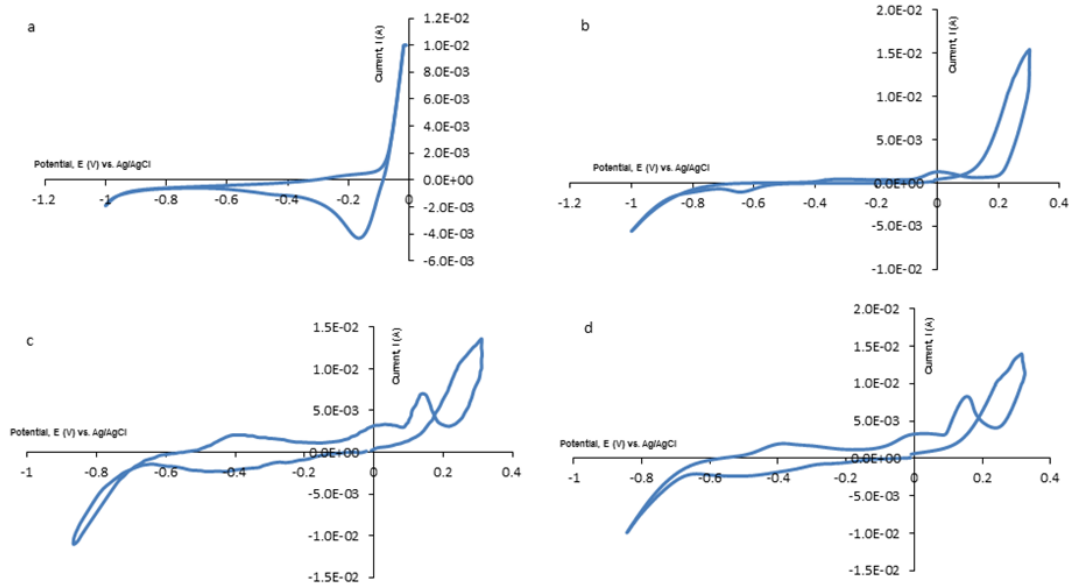


Fig 5: Cyclic Voltammogram of (a) Cu substrate (b) Bi-2.5Ag (c) Bi-2.5Ag + 0.1 wt% MWCNT (d) Bi-2.5Ag + 0.1 wt% MLG with scan rate of  $20 \text{ mVs}^{-1}$  at  $0.5\text{M KCl}$ .

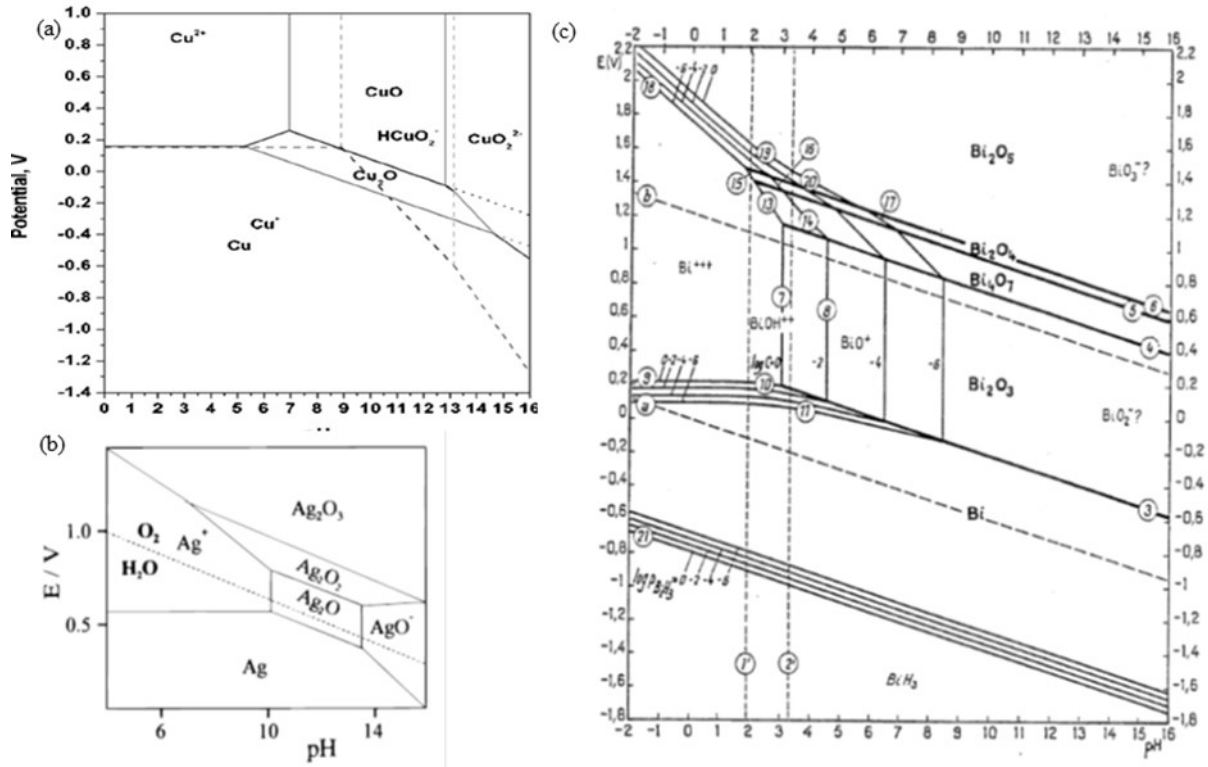


Fig 6: Pourbaix diagram of (a) copper (b) silver (c) bismuth

Table 1: Atomic weight, valency and the mass fraction of elements involved in the corrosion process.

Element /Compound symbol	Atomic weight (g)	Valency	Fraction
Bi	208.9	+3	65.96
Ag	107.8	+1	34.03
Bi - Ag	316.7		

### 3.2.2 Bi-2.5Ag and its reinforced systems corrosion rate

The polarization curves for samples at different buffer acids with pH 5 ( $\text{H}_2\text{SO}_4$ ,  $\text{HCl}$ ,  $\text{HNO}_3$ ) in Figure 7 exhibit polarization over potential ( $E_{\text{corr}}$ ) at the presence of various weight percentage of the reinforced nano particles in the solder matrix at the same acidic electrolyte. The results show that each reinforced matrix which was studied at different corrosive electrolyte had its specific  $E_{\text{corr}}$ .

The polarization peaks of the reinforced sample with MWCNT in  $\text{H}_2\text{SO}_4$  media (Fig 7(a)) demonstrated that the  $E_{\text{corr}}$  for 0.01 and 0.03 wt% occurred at more positive over-potential values than the matrix. However, by increasing the amount of MWCNT in the matrix, the  $E_{\text{corr}}$  is located at the smaller value than the matrix. Though,  $E_{\text{corr}}$  for 0.05 wt% has smaller over-potential value than others. For the samples which were reinforced with MLG at the same corrosive media  $E_{\text{corr}}$  for 0.03 and 0.05 wt% of MLG in matrix is set to a positive value, while for 0.01, 0.07 and 0.1 wt% of MLG, it is set to a smaller value (Fig 7(b)).

The  $E_{\text{corr}}$  peaks for the reinforced samples with MWCNT in  $\text{HCl}$  media are shown in Figure 7(c). All peaks were located at more positive over-potential values than the  $E_{\text{corr}}$  belonging to Bi-2.5Ag, except for the peak for the existence of 0.1 wt% of MWCNT in the matrix. On the other hand, the sample which is reinforced with MLG,  $E_{\text{corr}}$  values for 0.03 and 0.05 wt% of nano particles in the matrix are larger than the Bi-2.5Ag matrix. However, at the same media,  $E_{\text{corr}}$  values for 0.01, 0.07 and 0.1 wt% of MLG in the matrix are located at the smaller value (Fig 7(d)).

The  $E_{corr}$  peaks for the reinforced samples with MWCNT in  $HNO_3$  media were illustrated in Figure 7(e). As it can be seen only  $E_{corr}$  for 0.07 wt% MWCNT in Bi-2.5Ag situated at lower over-potential than the matrix and  $E_{corr}$  for all the other MWCNT weight percentages (0.01, 0.03, 0.05 and 0.1) located at a more positive value than the matrix. Indeed, for 0.05 and 0.1 wt%,  $E_{corr}$  values overlap with each other. With the same corrosive media, regarding the reinforced sample with MLG, all  $E_{corr}$  values for different weight percentage of this nano particle in the matrix are located at a more positive value than the plain matrix  $E_{corr}$  (Fig 7(f)). The polarization curve for the blank Cu substrate displayed in all the aforementioned figures shows its  $E_{corr}$  value in all three acids located at a higher positive value than Bi-2.5Ag and its composite alloys with MWCNT and MLG. This dissimilarity between  $E_{corr}$  values of blank Cu substrate and solder alloys (Bi-2.5Ag and Bi-2.5Ag+ MWCNT/MLG) melted on the Cu substrate confirmed that the Cu substrate was not directly involved in the process, even though the substrate indirectly affected the current density and the over-potential of the soldering alloys.

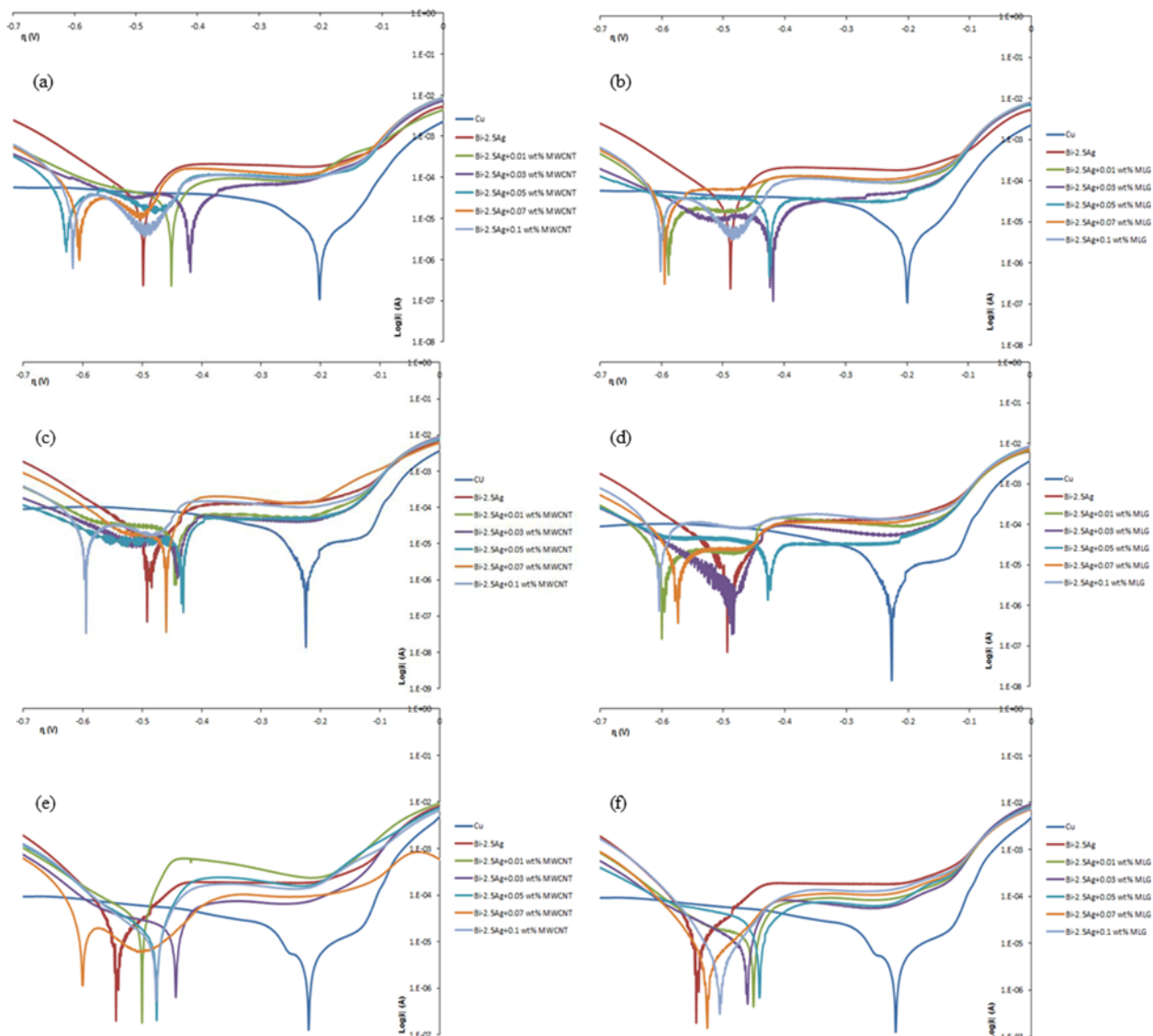


**Fig 7: Polarization curves for different weight percentage of nano particles in the solder matrix and different corrosive electrolytes. (a) MWCNT and  $H_2SO_4$  (b) MLG and  $H_2SO_4$  (c) MWCNT and HCl (d) MLG and HCl (e) MWCNT and  $HNO_3$  (f) MLG and  $HNO_3$ .**

The corrosion rate was calculated by using the equation 4. In this equation, the value of EW and the density were assessed as 79.36 and 19.81( $g/cm^3$ ) (the value of theoretical density), respectively. The rate of corrosion in the media with HCl (Fig 8 (a)) showed that the corrosion rate which is a function of  $i_{corr}$  also increased by increasing the amount of nano particles in the matrix. The corrosion rate increased from 1.693 (mm/yr) to 2.734 (mm/yr) and 2.552 (mm/yr) for MWCNT and MLG, respectively.

Figure 8(b) demonstrates the rate of corrosion for the samples in the corrosive electrolyte which contained  $\text{HNO}_3$ . It can be seen the corrosion rate increased by increasing the amount of nano particles in the matrix. The corrosion rate increased from 1.425 (mm/yr) for the pattern sample (the sample without reinforced particles) to 2.671 (mm/yr) for the sample reinforced with 0.1 wt% of MWCNT; while, the corrosion rate increased to 2.405 (mm/yr) for the sample reinforced with 0.1 wt% of MLG. It is obvious that the corrosion rate increased more for samples with MWCNT than the sample with MLG. The corrosion rates for the samples which were calculated for the electrolyte with  $\text{H}_2\text{SO}_4$  were shown in Figure 8(c). Regarding the corrosion rate which has a direct relation with  $i_{\text{corr}}$ , the corrosion rate also increased by increasing the  $i_{\text{corr}}$ . Hence, the maximum corrosion rate occurred at the existence of 0.1 wt% of nano particles in the matrix which is 2.539 (mm/yr) for MWCNT and 2.565 (mm/yr) for MLG, while the corrosion rate for the sample without reinforced particles is 1.358 (mm/yr). It should be mentioned that the corrosion rate for 0.01 wt% of nano particles, MWCNT corrosion rate was found as 1.509 (mm/yr) and for MLG as 1.493 (mm/yr) in this corrosive electrolyte.

From the extracted and computed  $i_{\text{corr}}$  and the corrosion rate values related to the different corrosive electrolytes which contained HCl,  $\text{HNO}_3$  and  $\text{H}_2\text{SO}_4$  as well as electrical conductivity of the corrosive electrolytes, it can be concluded that the corrosion rate of Bi-2.5Ag and its reinforced systems is affected by the conductivity of the solder alloy and the corrosive electrolyte. In section 3.1, it is comprehensively explained that by increasing the weight percentage of nano particles in the matrix, the electrical conductivity of composite Bi-2.5Ag increased. Also, it is explained that at the same weight percentage of nano particles in the matrix, MWCNT improved the conductivity of solder alloy more than MLG. Table 2 illustrates the electrical conductivity of corrosive electrolytes. It is shown that electrolyte with HCl has a better conductivity than one with  $\text{HNO}_3$  and electrolyte with  $\text{H}_2\text{SO}_4$  has less conductivity in comparison with the two other electrolytes.

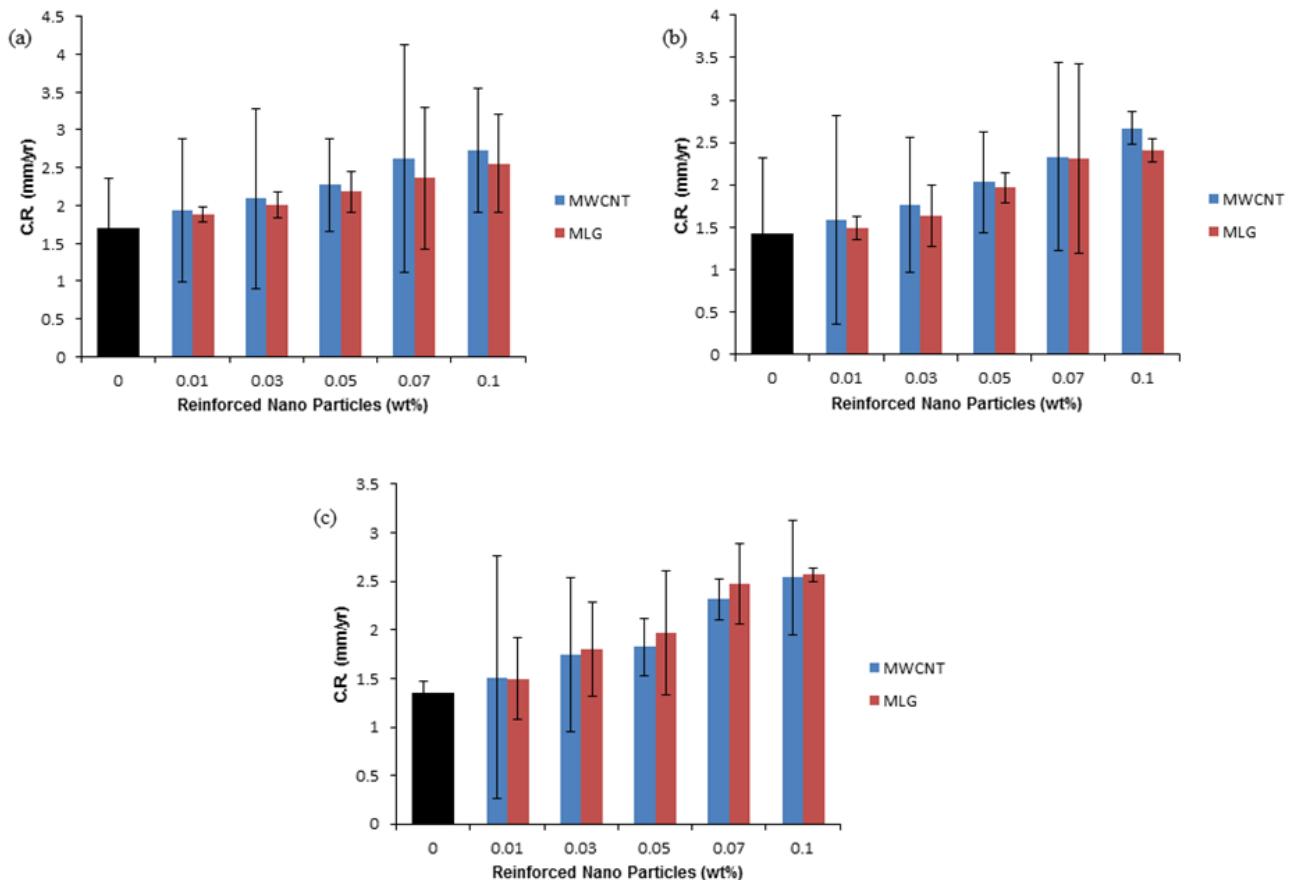


Fig 8: The estimated corrosion rates for reinforced sample with MWCNT and MLG at corrosive media which contained (a) HCl (b)  $\text{HNO}_3$  (c)  $\text{H}_2\text{SO}_4$ .

Table 2: Electrical conductivity of corrosive electrolytes (temperature coefficient 2.5 %/°C)

Electrolyte	pH ( $\pm 0.01$ )	Electrical Conductivity (mS/cm) ( $\pm 0.1$ )
0.5M KCl	6.42	41.6
0.5M KCl + HNO <sub>3</sub>	5.00	70.6
0.5M KCl + H <sub>2</sub> SO <sub>4</sub>	5.00	69.4
0.5M KCl + HCl	5.00	71.1

### 3.2.3 The passivation behavior Bi-2.5Ag and its reinforced systems

The extracted passivation potential ( $E_{pp}$ ), critical current ( $i_{cc}$ ) and passive current ( $i_p$ ) from Figure 9 are shown in Table 3 for Bi-2.5Ag and its composite systems with MWCNT and MLG at different corrosive electrolytes. By increasing the amount of nano particles in the solder matrix, the value of  $E_{pp}$ ,  $i_{cc}$  and  $i_p$  for the composite Bi-2.5Ag with MWCNT and MLG, increased in all the three corrosive electrolytes and shifted to more positive values.

Regarding the composite samples with MWCNT, the maximum value of passivation potential ( $E_{pp}$ ) which belongs to 0.1 wt% of nano particles in the solder matrix is  $1.171 \times 10^{-1}$  A for the corrosive electrolyte with HCl, and  $1.094 \times 10^{-1}$  A and  $8.728 \times 10^{-2}$  A for the corrosive electrolyte with HNO<sub>3</sub> and H<sub>2</sub>SO<sub>4</sub>, respectively. The  $E_{pp}$  for the composite sample with MLG for the electrolyte with H<sub>2</sub>SO<sub>4</sub>, in general, has smaller value than the sample with MWCNT, as  $8.193 \times 10^{-2}$  A for the corrosive electrolyte with H<sub>2</sub>SO<sub>4</sub>, while for electrolytes with HCl and HNO<sub>3</sub> has a bigger value as  $8.834 \times 10^{-2}$  A and  $9.368 \times 10^{-2}$  A, respectively. For the sample without reinforced particles, in the same electrolytes, the  $E_{pp}$  values are  $6.698 \times 10^{-2}$  A,  $5.553 \times 10^{-2}$  A and  $6.339 \times 10^{-2}$  A for corrosive electrolytes containing H<sub>2</sub>SO<sub>4</sub>, HCl and HNO<sub>3</sub>.

According to Table 3, the maximum critical current ( $i_{cc}$ ) in all three corrosive electrolytes occurred while the sample contained 0.1 wt% of MWCNT at the corrosive electrolyte contained HCl as  $4.185 \times 10^{-3}$  A, while the  $i_{cc}$  for composite sample with MLG with the same weight percentage of nano particles is  $1.964 \times 10^{-3}$  A. The maximum value of  $i_{cc}$  for the composite sample with MWCNT and MLG in electrolyte which contained H<sub>2</sub>SO<sub>4</sub> are  $1.953 \times 10^{-3}$  A and  $1.614 \times 10^{-3}$  A, and in electrolyte which contained HNO<sub>3</sub> are  $3.001 \times 10^{-3}$  A and  $2.998 \times 10^{-3}$  A, respectively. For the sample, without the reinforced nano particles the value of  $i_{cc}$  (the minimum value) is  $2.417 \times 10^{-4}$  A,  $3.081 \times 10^{-4}$  A and  $3.768 \times 10^{-4}$  A for the corrosive electrolytes which contained H<sub>2</sub>SO<sub>4</sub>, HNO<sub>3</sub> and HCl, respectively.

The passive current ( $i_p$ ) trend has the same manner as  $E_{pp}$  and  $i_{cc}$  which shows by increasing the amount of reinforced nano particles in the matrix the value of  $i_p$  also increased. The  $i_p$  value increased from  $1.303 \times 10^{-3}$  A,  $1.225 \times 10^{-3}$  A and  $1.239 \times 10^{-3}$  A for Bi-2.5Ag at the corrosive electrolyte which contained H<sub>2</sub>SO<sub>4</sub>, HCl and HNO<sub>3</sub>. The maximum  $i_p$  for the reinforced sample with 0.1 wt% of MWCNT at the electrolyte which contained H<sub>2</sub>SO<sub>4</sub>, HCl and HNO<sub>3</sub> are  $2.470 \times 10^{-3}$  A,  $4.207 \times 10^{-3}$  A and  $3.634 \times 10^{-3}$  A at the same electrolytes the values of  $i_p$  for 0.1 wt% of MLG are  $2.493 \times 10^{-3}$  A,  $2.520 \times 10^{-3}$  A and  $3.623 \times 10^{-3}$  A. Indeed, the composite sample with 0.1 wt% of MWCNT sample has the maximum  $i_p$  among all the samples.

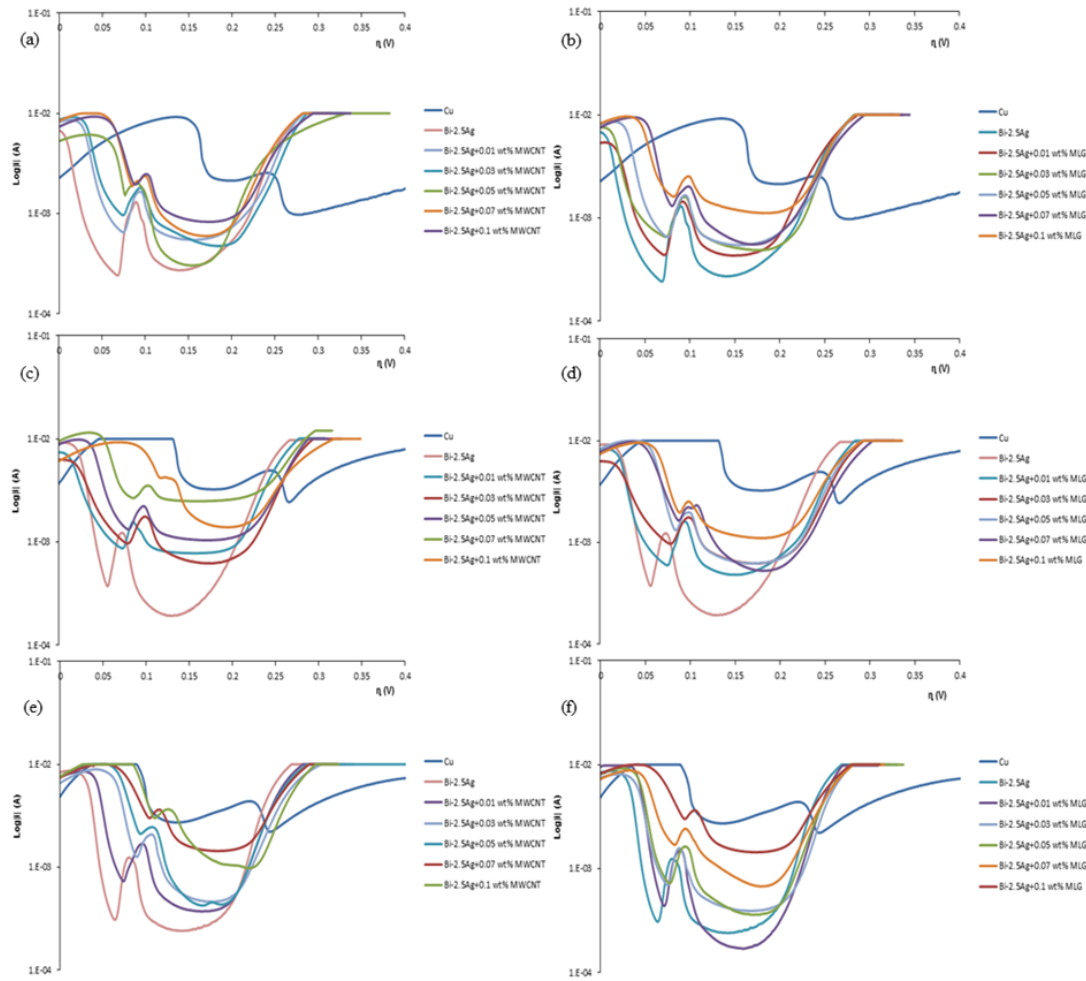


Fig 9: The behavior of active-passive layer for different weight percentage nano particles in the solder matrix and different corrosive electrolytes (a) MWCNT and  $H_2SO_4$  (b) MLG and  $H_2SO_4$  (c) MWCNT and HCl (d) MLG and HCl (e) MWCNT and  $HNO_3$  (f) MLG and  $HNO_3$

Nano particle	MWCNT						MLG						
	Nano particle wt%	0.00	0.01	0.03	0.05	0.07	0.1	0.00	0.01	0.03	0.05	0.07	0.1
0.5 M KCl+ $H_2SO_4$	$E_{pp}$	6.805 $\times 10^{-2}$	7.342 $\times 10^{-2}$	7.348 $\times 10^{-2}$	7.582 $\times 10^{-2}$	8.407 $\times 10^{-2}$	8.728 $\times 10^{-2}$	6.805 $\times 10^{-2}$	7.032 $\times 10^{-2}$	7.232 $\times 10^{-2}$	7.659 $\times 10^{-2}$	7.873 $\times 10^{-2}$	8.193 $\times 10^{-2}$
	$i_{cc}$	2.417 $\times 10^{-4}$	6.515 $\times 10^{-4}$	9.619 $\times 10^{-4}$	1.522 $\times 10^{-3}$	1.887 $\times 10^{-3}$	1.953 $\times 10^{-3}$	2.417 $\times 10^{-4}$	4.388 $\times 10^{-4}$	6.533 $\times 10^{-4}$	6.668 $\times 10^{-4}$	1.323 $\times 10^{-3}$	1.614 $\times 10^{-3}$
	$i_p$	1.303 $\times 10^{-3}$	1.640 $\times 10^{-3}$	1.771 $\times 10^{-3}$	2.018 $\times 10^{-3}$	2.215 $\times 10^{-3}$	2.470 $\times 10^{-3}$	1.303 $\times 10^{-3}$	1.438 $\times 10^{-3}$	1.601 $\times 10^{-3}$	1.655 $\times 10^{-3}$	2.020 $\times 10^{-3}$	2.493 $\times 10^{-3}$
0.5 M KCl+ HCl	$E_{pp}$	5.553 $\times 10^{-2}$	7.339 $\times 10^{-2}$	7.873 $\times 10^{-2}$	8.087 $\times 10^{-2}$	8.553 $\times 10^{-2}$	1.171 $\times 10^{-1}$	5.553 $\times 10^{-2}$	7.446 $\times 10^{-2}$	7.766 $\times 10^{-2}$	8.407 $\times 10^{-2}$	8.666 $\times 10^{-2}$	8.834 $\times 10^{-2}$
	$i_{cc}$	5.316 $\times 10^{-4}$	8.675 $\times 10^{-4}$	9.667 $\times 10^{-4}$	1.328 $\times 10^{-3}$	2.666 $\times 10^{-3}$	4.185 $\times 10^{-3}$	5.316 $\times 10^{-4}$	6.079 $\times 10^{-4}$	9.667 $\times 10^{-4}$	1.314 $\times 10^{-3}$	1.654 $\times 10^{-3}$	1.964 $\times 10^{-3}$
	$i_p$	1.515 $\times 10^{-3}$	1.562 $\times 10^{-3}$	1.764 $\times 10^{-3}$	2.225 $\times 10^{-3}$	3.515 $\times 10^{-3}$	4.207 $\times 10^{-3}$	1.515 $\times 10^{-3}$	1.606 $\times 10^{-3}$	1.764 $\times 10^{-3}$	1.974 $\times 10^{-3}$	2.217 $\times 10^{-3}$	2.520 $\times 10^{-3}$
0.5 M KCl+ $HNO_3$	$E_{pp}$	6.339 $\times 10^{-2}$	7.339 $\times 10^{-2}$	8.834 $\times 10^{-2}$	9.262 $\times 10^{-2}$	1.036 $\times 10^{-1}$	1.094 $\times 10^{-1}$	6.339 $\times 10^{-2}$	7.159 $\times 10^{-2}$	7.446 $\times 10^{-2}$	7.766 $\times 10^{-2}$	8.300 $\times 10^{-2}$	9.368 $\times 10^{-2}$
	$i_{cc}$	3.081 $\times 10^{-4}$	7.302 $\times 10^{-4}$	1.261 $\times 10^{-4}$	2.116 $\times 10^{-4}$	2.998 $\times 10^{-3}$	3.001 $\times 10^{-3}$	3.081 $\times 10^{-4}$	4.405 $\times 10^{-4}$	6.964 $\times 10^{-4}$	7.235 $\times 10^{-4}$	1.692 $\times 10^{-3}$	2.998 $\times 10^{-3}$
	$i_p$	1.239 $\times 10^{-3}$	1.687 $\times 10^{-3}$	2.080 $\times 10^{-3}$	2.446 $\times 10^{-3}$	3.629 $\times 10^{-3}$	3.634 $\times 10^{-3}$	1.239 $\times 10^{-3}$	1.459 $\times 10^{-3}$	1.570 $\times 10^{-3}$	1.627 $\times 10^{-3}$	2.416 $\times 10^{-3}$	3.623 $\times 10^{-3}$
		$10^{-3}$	$10^{-3}$	$10^{-3}$	$10^{-3}$	$10^{-3}$	$10^{-3}$	$10^{-3}$	$10^{-3}$	$10^{-3}$	$10^{-3}$	$10^{-3}$	$10^{-3}$

Table 3:  $E_{pp}$  [ $\pm 0.01-0.1$ ],  $i_{cc}$  [ $\pm 0.0001-0.001$ ] and  $i_p$  [ $\pm 0.001$ ] for Bi-2.5Ag and its composite system with MWCNT and MLG at different corrosive electrolytes (pH 5)

## 4. Conclusion

1. It was found that for both reinforced nano particles in the matrix the electrical resistivity of Bi-2.5Ag decreased; while, the effect of MWCNT on the electrical resistivity of the solder matrix was more than MLG. The electrical resistivity of Bi-2.5Ag decreased from 3.67 ( $\mu\Omega\cdot\text{cm}$ ) to 2.38 ( $\mu\Omega\cdot\text{cm}$ ) and 2.96 ( $\mu\Omega\cdot\text{cm}$ ) for MWCNT and MLG, respectively, when there was 0.01 wt% of nano particles in the matrix. The maximum decrease of resistivity was observed for the sample with 0.1 wt% of nano particles which is 1.89 ( $\mu\Omega\cdot\text{cm}$ ) for MWCNT and 2.53 ( $\mu\Omega\cdot\text{cm}$ ) for MLG. It was also deduced that the electrical behavior is at function of the surface area and the quality of each reinforcement particles.

2. The corrosion behavior of Bi-2.5Ag and its composites with MWCNT and MLG was investigated by an electrochemical technique. In general, adding MWCNT and MLG to Bi-2.5Ag increased the corrosion rate. The results from the Tafel plot curves which were run in three different acidic electrolytes show that the corrosion rate is a function of the electrical conductivity of the sample, the electrical conductivity of electrolyte and the number of  $\text{H}^+$  in the corrosive electrolyte.

It can be concluded,  $E_{\text{corr}}$  for the soldering alloys is affected by different weight percentages of the reinforcement nano particles in the solder matrix at each corrosive electrolyte. For instance, for the same corrosive electrolyte,  $E_{\text{corr}}$  is different by changing the amount of the nanoparticle.

The results demonstrate that the corrosion rate increased by increasing the amount of nano particles in the solder matrix in all three corrosive electrolytes. For the electrolyte which contained HCl and  $\text{HNO}_3$ , the samples reinforced with MWCNT, the corrosion rate has a bigger value. It is also observed that the rate of corrosion is bigger in the electrolyte with HCl than  $\text{HNO}_3$  for both reinforced samples with MWCNT and MLG. However, the reinforced sample with MLG has a bigger corrosion value than MWCNT in the electrolyte which contained  $\text{H}_2\text{SO}_4$  while the amounts of nano particles were the same in the solder matrix. This behavior can be attributed to the existence of two  $\text{H}^+$  of  $\text{H}_2\text{SO}_4$  in the corrosive electrolyte. Overall, the rate of corrosion determines the behavior of the active-passive layer. Regarding that, the value of  $E_{\text{pp}}$ ,  $i_{\text{cc}}$  and  $i_{\text{p}}$  follow the trend of corrosion rate and by increasing the amount of nano particles in the solder matrix, the corrosion rate increased in its selected corrosive electrolytes. It can be concluded that the  $E_{\text{pp}}$ ,  $i_{\text{cc}}$  and  $i_{\text{p}}$  are also affected by the conductivity of the sample, the conductivity of corrosive electrolyte and the number of  $\text{H}^+$  in the corrosive electrolyte.

## Conflict of Interest

The authors declare no conflict of interest.

## Acknowledgement

The authors would like to acknowledge Universiti Putra Malaysia (UPM) (UPM-GRANT Putra, UPM/GP-IPB/2020/9688700) for providing necessary resources and facilities in completing this study.

## References

1. Wu, X., et al. The improvements of high temperature Zn-based lead free solder. in Electronic Components and Technology Conference (ECTC), 2015 IEEE 65th. 2015: IEEE.
2. Raj, A., et al. Proportional Hazard Model of doped low creep lead free solder paste under thermal shock. in Thermal and Thermomechanical Phenomena in Electronic Systems (ITherm), 2016 15th IEEE Intersociety Conference on. 2016: IEEE.
3. Dele-Afolabi, T., et al., Investigating the effect of isothermal aging on the morphology and shear strength of Sn-5Sb solder reinforced with carbon nanotubes. *Journal of Alloys and Compounds*, 2015. 649: p. 368-374.
4. Dele-Afolabi, T., et al., Growth kinetics of intermetallic layer in lead-free Sn-5Sb solder reinforced with multi-walled carbon nanotubes. *Journal of Materials Science: Materials in Electronics*, 2015. 26(10): p. 8249-8259.
5. Knickerbocker, J.U., et al. 3D silicon integration. in Electronic Components and Technology Conference, 2008. ECTC 2008. 58th. 2008: IEEE.
6. Kang, S.K. and A.K. Sarkhel, Lead (Pb)-free solders for electronic packaging. *Journal of Electronic Materials*, 1994. 23(8): p. 701-707.
7. Chidambaram, V., J. Hattel, and J. Hald, High-temperature lead-free solder alternatives. *Microelectronic Engineering*, 2011. 88(6): p. 981-989.
8. Suganuma, K., Advances in lead-free electronics soldering. *Current Opinion in Solid State and Materials Science*, 2001. 5(1): p. 55-64.
9. Suganuma, K., S.-J. Kim, and K.-S. Kim, High-temperature lead-free solders: Properties and possibilities. *JOM Journal of the Minerals, Metals and Materials Society*, 2009. 61(1): p. 64-71.
10. Manikam, V.R. and K.Y. Cheong, Die attach materials for high temperature applications: A review. *IEEE Transactions on Components, Packaging and Manufacturing Technology*, 2011. 1(4): p. 457-478.

11. Hampshire, W.B., The search for lead-free solders. *Soldering & Surface Mount Technology*, 1993. 5(2): p. 49-52.
12. Cheng, S., C.-M. Huang, and M. Pecht, A review of lead-free solders for electronics applications. *Microelectronics Reliability*, 2017. 75: p. 77-95.
13. Shimoda, M., et al., Effects of Ag Content on the Mechanical Properties of Bi-Ag Alloys Substitutable for Pb based Solder. *Transactions of JWRI*, 2012. 41(2): p. 51-54.
14. Lalena, J.N., N.F. Dean, and M.W. Weiser, Experimental investigation of Ge-doped Bi-11Ag as a new Pb-free solder alloy for power die attachment. *Journal of Electronic Materials*, 2002. 31(11): p. 1244-1249.
15. Spinelli, J.E., B.L. Silva, and A. Garcia, Microstructure, phases morphologies and hardness of a Bi-Ag eutectic alloy for high temperature soldering applications. *Materials & Design*, 2014. 58: p. 482-490.
16. Song, J.-M., H.-Y. Chuang, and T.-X. Wen, Thermal and tensile properties of Bi-Ag alloys. *Metallurgical and Materials Transactions A*, 2007. 38(6): p. 1371-1375.
17. Song, J.-M., H.-Y. Chuang, and Z.-M. Wu, Interfacial reactions between Bi-Ag high-temperature solders and metallic substrates. *Journal of Electronic Materials*, 2006. 35(5): p. 1041-1049.
18. Song, J.-M., H.-Y. Chuang, and Z.-M. Wu, Substrate dissolution and shear properties of the joints between Bi-Ag alloys and Cu substrates for high-temperature soldering applications. *Journal of Electronic Materials*, 2007. 36(11): p. 1516-1523.
19. Allaoui, A., et al., Mechanical and electrical properties of a MWNT/epoxy composite. *Composites Science and Technology*, 2002. 62(15): p. 1993-1998.
20. Tang, Y., G. Li, and Y. Pan, Effects of TiO<sub>2</sub> nanoparticles addition on microstructure, microhardness and tensile properties of Sn-3.0 Ag-0.5 Cu-xTiO<sub>2</sub> composite solder. *Materials & Design*, 2014. 55: p. 574-582.
21. Tsao, L., et al., Effects of nano-Al<sub>2</sub>O<sub>3</sub> particles on microstructure and mechanical properties of Sn<sub>3</sub>.5Ag<sub>0</sub>.5Cu composite solder ball grid array joints on Sn/Cu pads. *Materials & Design*, 2013. 50: p. 774-781.
22. Xu, S., et al., Interfacial intermetallic growth and mechanical properties of carbon nanotubes reinforced Sn<sub>3</sub>.5Ag<sub>0</sub>.5Cu solder joint under current stressing. *Journal of Alloys and Compounds*, 2014. 595: p. 92-102.
23. Dele-Afolabi, T., et al., Physical and mechanical properties enhancement of lead free solders reinforced with carbon nanotubes: a critical review. *Advances in Environmental Biology*, 2014: p. 2600-2609.
24. Yang, Z., W. Zhou, and P. Wu, Effects of Ni-coated carbon nanotubes addition on the microstructure and mechanical properties of Sn-Ag-Cu solder alloys. *Materials Science and Engineering: A*, 2014. 590: p. 295-300.
25. Gancarz, T., et al., Effect of Ag addition to Zn-12Al alloy on kinetics of growth of intermediate phases on Cu substrate. *Journal of Alloys and Compounds*, 2014. 582: p. 313-322.
26. Nai, S., J. Wei, and M. Gupta, Improving the performance of lead-free solder reinforced with multi-walled carbon nanotubes. *Materials Science and Engineering: A*, 2006. 423(1): p. 166-169.
27. Gojny, F.H., et al., Influence of nano-modification on the mechanical and electrical properties of conventional fibre-reinforced composites. *Composites Part A: Applied Science and Manufacturing*, 2005. 36(11): p. 1525-1535.
28. Gojny, F.H., et al., Evaluation and identification of electrical and thermal conduction mechanisms in carbon nanotube/epoxy composites. *Polymer*, 2006. 47(6): p. 2036-2045.
29. Wu, H., et al., Properties investigation on isotropical conductive adhesives filled with silver coated carbon nanotubes. *Composites Science and Technology*, 2007. 67(6): p. 1182-1186.
30. Chen, G., et al., Effects of fullerenes reinforcement on the performance of 96.5 Sn-3Ag-0.5 Cu lead-free solder. *Materials Science and Engineering: A*, 2015. 636: p. 484-492.
31. Chen, G., et al., Microstructures and properties of new Sn-Ag-Cu lead-free solder reinforced with Ni-coated graphene nanosheets. *Journal of Alloys and Compounds*, 2016. 656: p. 500-509.
32. Xu, L., et al., Effect of graphene nanosheets on the corrosion behavior of Sn-Ag-Cu solders. *Journal of Materials Science: Materials in Electronics*, 2015. 26(8): p. 5625-5634.
33. Nai, S., J. Wei, and M. Gupta, Effect of carbon nanotubes on the shear strength and electrical resistivity of a lead-free solder. *Journal of Electronic Materials*, 2008. 37(4): p. 515-522.
34. Ghamarian, N., et al., Photocorrosion of CuInSe<sub>2</sub> Thin Film by Electrochemical Polarization in Acidic and Alkaline Medium. *Int. J. Electrochem. Sci*, 2013. 8: p. 5161-5171.
35. Fontana, M.G., *Corrosion engineering*. 2005: Tata McGraw-Hill Education.
36. Djellal, L., et al., Photoelectrochemical hydrogen-evolution over p-type chalcopyrite CuInSe<sub>2</sub>. *Journal of Alloys and Compounds*, 2009. 476(1): p. 584-589.

37. Shi, Y., X. Wei, and B. Tolla, Smart chemistry towards highly efficient soldering material formulation. Proceedings of SMTA International, Rosemont, 2014: p. 436-443.
38. Qu, G., et al., Nonaqueous Halide-Free Flux Reactions with Tin-Based Solders. Journal of Electronic Materials, 2015. 44(4): p. 1144-1150.
39. Burda, M., et al., Soldering of carbon materials using transition metal rich alloys. ACS nano, 2015. 9(8): p. 8099-8107.
40. Luo, J., et al., Electrically conductive adhesives based on thermoplastic polyurethane filled with silver flakes and carbon nanotubes. Composites Science and Technology, 2016(129): p. 191-197.
41. Lalwani, G., W. Xing, and B. Sitharaman, Enzymatic degradation of oxidized and reduced graphene nanoribbons by lignin peroxidase. Journal of Materials Chemistry B, 2014. 2(37): p. 6354-6362.
42. Ferrari, A.C. and D.M. Basko, Raman spectroscopy as a versatile tool for studying the properties of graphene. Nature nanotechnology, 2013. 8(4): p. 235-246.

**Citation:** M.A Azmah Hanim et al. "Electrical and corrosion characterisation of nano-composite eutectic Bi-Ag solder alloy reinforced with multi-wall carbon nanotube and multi-layer graphene ". SVOA Materials Science &Technology 2:3 (2020) 62-75.

**Copyright:** © 2020 All rights reserved by M.A Azmah Hanim et al. This is an open access article distributed under the Creative Commons Attribution License, which permits unrestricted use, distribution, and reproduction in any medium, provided the original work is properly cited.